Chemical Influence of the Dianhydride and the Diamine Structure on a Series of Copolyimides Studied by Molecular Dynamics Simulations

E. Pinel,† D. Brown,† C. Bas,† R. Mercier,‡ N. D. Albérola,† and S. Neyertz*,†

Laboratoire Matériaux Organiques à Propriétés Spécifiques (LMOPS), UMR CNRS 5041, Université de Savoie, Bât. IUT, 73376 Le Bourget du Lac Cedex, France, and BP 24, 69390 Vernaison, France

Received June 17, 2002; Revised Manuscript Received October 8, 2002

ABSTRACT: Molecular dynamics (MD) simulations are undertaken on a series of five copolyimides based on two different dianhydrides: the flexible 4,4′-oxydiphthalic dianhydride (ODPA) and the rigid bulky bicyclo(2.2.2)-oct-7-ene-2,3,5,6-tetracarboxylic dianhydride (BCDA). The diamines are respectively 4,4′-oxydi(phenylamine) (ODA), 2-trifluoride-4,4′-oxydi(phenylamine) (CF_3ODA) and 2-methoxy-4,4′-oxydi-(phenylamine) (MeOODA). These are potential candidates for gas separation membranes, and the effects of increasing BCDA content in ODPA/BCDA copolyimides as well as adding trifluoromethyl or methoxy substituents on the ODA are studied at the molecular level. Amorphous long-chain models are built using a hybrid pivot Monte Carlo/MD sampling preparation procedure. The reproducibility of this approach is tested on a series of eight independently prepared systems. Densities, cohesive energies, Hildebrand parameters, conformational characteristics, intermolecular structures, and the available void spaces are analyzed for each system under study. Both the BCDA moiety and the trifluoromethyl substituent on the diamine are found to have similar consequences on the properties of the copolyimide by decreasing chain cohesion and increasing the available void space. This is related to the steric effect of the BCDA dianhydride, while the trifluoromethyl combines both steric and electronic repulsion. The steric effect of the methoxy substituent on the diamine is not strong enough to significantly differ from the unsubstituted system.

1. Introduction

Polyimides are high-performance macromolecules which are usually obtained via polycondensation of aromatic and/or alicylic dianhydride and diamine structures. They exhibit excellent mechanical and electrical characteristics over a large range of temperatures, as well as good chemical and long-term stabilities. They are also well-known for their separation properties, both with respect to gases and liquids. Their applications are manyfold and range from electronics, electrical engineering and aviation to filtration membranes.[1,2]

For many years now, much effort has been dedicated toward studying the relationships between the choice of the basic monomers and the resulting properties of the synthesized homopolyimides or copolyimides.[1−3] Experimental characterizations include density and solubility determinations as well as thermal, mechanical and permeation analyses. Polyimides have also been studied using UV/vis spectrophotometry,[4] wide-angle X-ray diffraction,[5,6] or even positron annihilation.[7,8] Within this context, it is interesting to add molecular dynamics (MD) simulations,[9] which are able to provide a dynamic model of the polyimide under study at the molecular level. This information can be used either to complement and interpret experimental evidence or to predict the properties of new polyimide structures prior to their synthesis.[10]

MD simulations have already been reported for several amorphous polyimides. Structural features of polyimides based on the BTDA (3,3′,4,4′-benzophenonetetracarboxylic) dianhydride and the DMDA (2,2-dimethyl-1,3-(4-aminophenoxy)propane) diamine in the bulk were compared to those of the same chains in vacuo.[11,12] The effect of the diamine on the overall flexibility and the mechanical properties of BTDA-based polyimides was assessed by studying four other diamines.[13] In both cases, a large number of structural properties such as radial distribution functions or ring correlation functions, torsion angle distributions, characteristic ratio, elastic moduli or yield strains could be obtained from the models.[11−13] A similar attempt was carried out on perylene-containing polyimides in order to characterize the degree of intra- and intermolecular nematic order.[14] Other applications of MD simulations to these systems include the transport of small gas molecules in polyimide matrixes[15−20] as well as the alignment of liquid crystal molecules on polyimide layers.[21−23] MD has also been used as a tool to complement scanning tunneling microscopy images of polyimide Langmuir−Blodgett films[24] and X-ray diffraction studies,[5,6] as well as modeling the poling process in piezoelectric polyimides.[25]

In the present work, a series of five copolyimides for potential membrane separation applications are considered. The polymers under study are based on two different dianhydrides, i.e., the flexible 4,4′-oxydiphthalic dianhydride (ODPA) and the rigid bicyclo-(2.2.2)-oct-7-ene-2,3,5,6-tetracarboxylic dianhydride (BCDA). The diamines are respectively 4,4′-oxydi(phenylamine) (ODA), 2-trifluoride-4,4′-oxydi(phenylamine) (CF_3ODA), and 2-methoxy-4,4′-oxydi(phenylamine) (MeOODA).

Our first goal is to assess the effect of increasing BCDA content in ODPA/BCDA copolyimides. Indeed, the bulky structure of the BCDA moiety makes it a very strong candidate to favor the transport of small molecules in polyimide systems. However, too much BCDA will lead to problems at the processing stage and its amount within a copolyimide will thus have to be

* Corresponding author.
† Université de Savoie.
‡ BP 24.

10.1021/ma020942j CCC: $22.00
Published on Web 11/27/2002

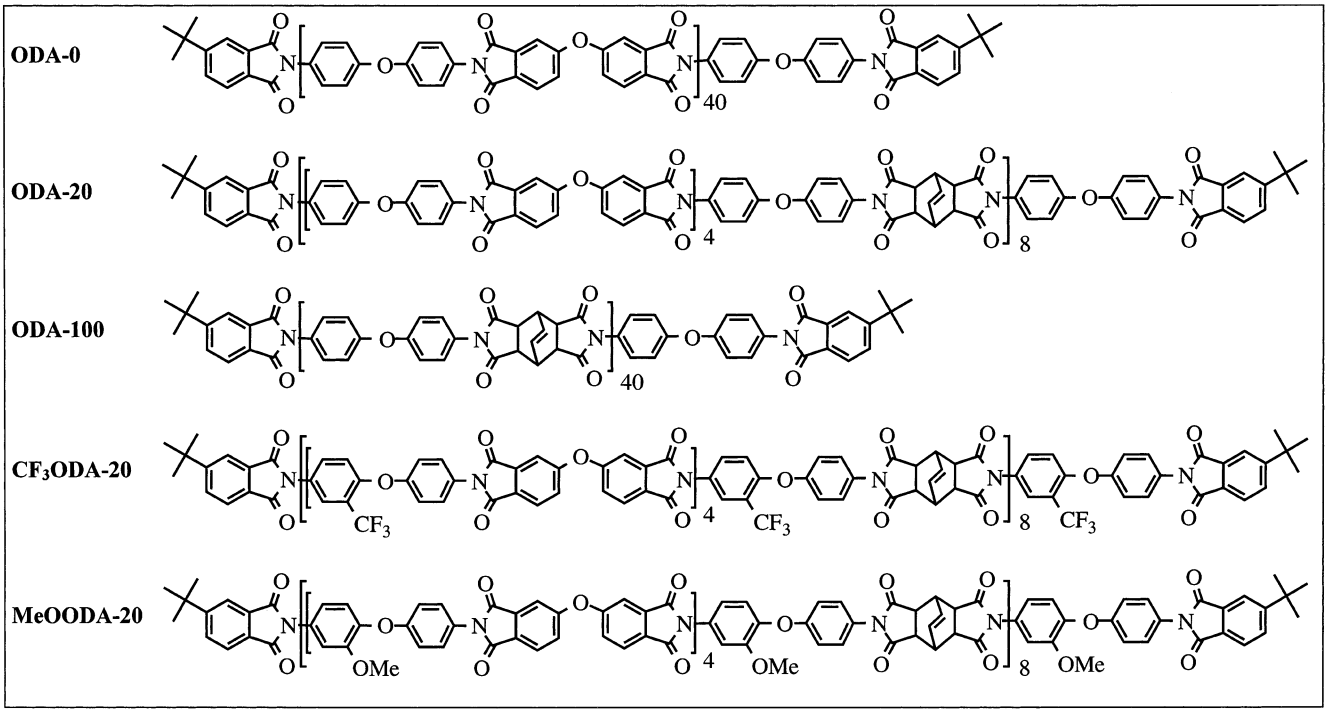

Figure 1. The five chemical structures under study as determined from experimental ^{1}H NMR characterizations.

limited. The second goal is then to study whether a substituent on the ODA diamine such as a trifluoromethyl or a methoxy group could have similar consequences at the molecular level and increase for example the available void space in these systems.

Five atomistic models are thus built and simulated in order to get an insight into the way the chemical structures and sequences of the monomers will affect the microscopic and macroscopic properties of these copolyimides and, in particular, lead to characteristics able to improve the transport of small molecules for use in separation membranes. Four of these copolyimides have already been synthesized and characterized,[26,27] and there is thus consistent experimental evidence available to confront our MD simulations.

We give the computational details of the model in section 2 while the results are given and discussed in section 3.

2. Computational Details

As stated above, the copolyimides under study have both been synthesized and characterized prior to the molecular dynamics simulations reported in this work,[26,27] with the exception of the methoxy-substituted system. Many features of the models have thus been chosen in order to correspond to experimental data. Details on the synthesis and characterization of the different systems have already been explicitely given elsewhere.[26] However, experimental evidence will be referred to whenever appropriate in order to discuss and complement the information at the molecular level.

All MD simulations were performed using the parallel version of the *gmq* program,[28] *ddgmq*,[29] on the CRAY T3E of the IDRIS supercomputing center (Orsay, France) and the SGi ORIGIN 2000 of the CINES supercomputing center (Montpellier, France), as well as a COMPAQ DS20E at the University of Savoie (Le Bourget-du-Lac, France).

2.1. Chemical Structures. The chemical structures of the copolyimides are all shown in Figure 1. For clarity, we will use the following names to distinguish the five systems: (a) "ODA-0" = the (ODPA−ODA) homopolyimide; (b) "ODA-20" = a regular (ODPA−ODA/BCDA−ODA) copolyimide with 20% BCDA; (c) "ODA-100" = the (BCDA−ODA) homopolyimide; (d) "CF_3ODA-20" = a regular (ODPA−CF_3ODA/BCDA−CF_3ODA) copolyimide with 20% BCDA; (e) "MeOODA-20" = a regular (ODPA−MeOODA/BCDA−MeOODA) copolyimide with 20% BCDA.

The limited amount of the BCDA moiety in the ODPA/BCDA copolyimides is related to experimental considerations. Indeed, we have shown that, although BCDA improves the solubility of these copolyimides, their glass-transition temperature also increases with higher BCDA contents and gets closer to their degradation temperature, which can lead to problems in the film processing stage.[26,27] Another word of caution is in order concerning the BCDA moiety. Although three isomeric forms are in principle possible (boat−boat, boat−chair, chair−chair), these are noninterconvertible once the monomer is formed. To our knowledge, no experimental evidence exists concerning the proportions of the different isomeric forms, and we have not been able to distinguish either their relative amount or sequence along the chains using NMR spectroscopy. A series of molecular mechanics calculations on single ODA−BCDA−ODA model oligomers were then carried out using a variety of commonly used force fields,[30] and they all gave the boat−boat conformer as the lowest energy form. As such, the boat−boat form of the BCDA moiety was exclusively used in the models.

^{1}H NMR characterization showed that the experimental chains contain an average of forty (dianhydride−diamine) units, and that the copolyimides with 20% BCDA have regular (ODPA−diamine)$_4$−(BCDA−diamine) sequences.[26,27] They are terminated at both ends by a 4-*tert*-butyl phthalic anhydride (PAtBu) and have a number-averaged molar mass of 20 000 g mol^{-1}. Although less ordered structures were also detected, the model chains were all built with forty (dianhydride−

diamine) and terminated as stated above (Figure 1). The number of atoms per chain of 40 (dianhydride−diamine) units is 2075 for ODA-0, 2051 for ODA-20, 1955 for ODA-100, 2174 for CF_3ODA-20, and 2215 for MeOODA-20. A chain was created for each system using equilibrium bond lengths, bend and dihedral angles.[31]

2.2. Potential. The force-field describes the potential energy of a system as a superposition of simple analytical functions which are presented in this section.

High-frequency vibrational bond stretching modes were removed according to the SHAKE routine,[32] with a relative tolerance of 10^{-6}, to allow for the use of a reasonable time step. All bond lengths were rigidly constrained to standard values.[31]

The functional form of the potential used in this study is

$$U_{\text{pot}} = \sum_{\theta} U_{\text{bend}}(\theta) + \sum_{\tau} U_{\text{tors}}(\tau) + \sum_{i\text{-sp}^2} U_{\text{oop}}(i) + \sum_{(i,j)_{\text{nb}}} U_{\text{LJ}}(|\mathbf{r}_{ij}|) + \sum_{(i,j)_{\text{nb}}} U_{\text{coul}}(|\mathbf{r}_{ij}|) \quad (1)$$

where (A) the first term describes the polymer angle-bending deformations by a harmonic function in the cosine of the bond angles, θ

$$U_{\text{bend}}(\theta) = \frac{k_\theta}{2}(\cos\theta - \cos\theta_0)^2 \quad (2)$$

(B) the second term represents the torsional motions around the dihedral angles τ by a sixth-order polynomial in $\cos\tau$

$$U_{\text{tors}}(\tau) = \sum_{n=0}^{6} a_n \cos^n\tau \quad (3)$$

(C) the third term keeps sp^2 structures planar by using a harmonic function in the distance d from the i-sp^2 atom to the plane defined by its three attached atoms

$$U_{\text{oop}}(i\text{-sp}^2) = \frac{k_{\text{oop}}}{2} d^2 \quad (4)$$

(D) the fourth term describes excluded-volume interactions between atoms belonging to the same molecule (but separated by more than two bonds) as well as atoms belonging to different molecules through the Lennard-Jones form of the van der Waals potential

$$U_{\text{LJ}}(|\mathbf{r}_{ij}|) = 4\,\epsilon_{ij}\left(\left(\frac{\sigma_{ij}}{|\mathbf{r}_{ij}|}\right)^{12} - \left(\frac{\sigma_{ij}}{|\mathbf{r}_{ij}|}\right)^{6}\right) \quad (5)$$

and (E) the fifth term accounts for Coulombic interactions under the same conditions as point D, with q_i and q_j being charges on atoms i and j, respectively, and ϵ_0 being the vacuum permittivity

$$U_{\text{coul}}(|\mathbf{r}_{ij}|) = \frac{q_i\, q_j}{4\pi\epsilon_o|\mathbf{r}_{ij}|} \quad (6)$$

The long-range effect of the electrostatic potential was taken into account by the Ewald summation method,[33,34] in order to perform the infinite sum of partial charges distributed in a periodic system.

Parameters for eqs 2−5 were directly derived from the TRIPOS 5.2 force-field,[31] since this force-field has been tested on a large number of cyclic compounds. The ϵ_{ij} and σ_{ij} cross-terms for the van der Waals parameters (eq 5) were obtained from the geometric mean of ϵ_{ii} and ϵ_{jj} and from the arithmetic mean of σ_{ii} and σ_{jj}. The charges used in eq 6 were obtained by performing ab initio calculations on a series of 27 representative fragments of the studied structures with Gaussian98[35] at the B3LYP/6-31G** level. Partial charges, q_i/e, were then extracted by an electrostatic potential (ESP) fitting procedure.[36] Only those charges taken from the central moieties of the model fragments were used in the subsequent MD simulations. All partial charges relating to our models are available as additional material.

2.3. Packing Models for the Chains. The preparation of dense samples for stiff long-chain polymers is an ongoing problem.[16,18,37] Indeed, the nanosecond time scale routinely accessible to classical MD simulations is far too short compared to configurational relaxation times in high molecular weight polymers,[38] and the starting structures for simulations of amorphous polymer chains must thus already be fairly relaxed. As it has been shown that growing into an ever decreasing volume and at low density with subsequent densification could introduce a bias in the chain statistics,[39,40] we have developed a generation procedure which allows samples to be grown directly at the density desired and with conformations expected from the equilibrium melt at the required temperature.[41] This so-called "hybrid PMC/MD technique" combines a single-chain sampling procedure, based on pivot Monte Carlo moves for rotatable torsions, with standard molecular dynamics algorithms, which are very good at exploring the various oscillatory modes of the chains. It is also based on the local energy approximation of Flory,[42] i.e., that the configurations of chains in the pure melt can be described by considering isolated molecules with only a certain number of specific near-neighbor intramolecular interactions.

The strength of this technique is that it has now been thoroughly tested on chain lengths for which full relaxation and equilibrium data can be achieved in a reasonable MD simulation time. The comparison between configurational statistics of chains obtained using single-chain PMC/MD sampling and those in the corresponding bulk melt have been carried out on a variety of short-chain homologues for *n*-alkanes,[41,43,44] poly(ethylene oxide) (PEO),[45,46] poly(vinyl chloride) (PVC),[47] poly(ether ether ketone) (PEEK), and two polyimides based on the BCDA and ODPA dianhydrides.[48] In most of these tests, the radii of gyration, end-to-end distances, and percentage of trans conformers of the chains were found to agree within over ∼95%. The only exceptions to date are the PEO homologues with a ∼70−80% agreement between single-chain-sampled and bulk melt configurations.[45,46] This discrepancy was eventually traced to a competition between intra- and intermolecular C−H···O interactions in the bulk melt,[47] which is obviously difficult to take into account using a Flory-type approach. It is worth noting too that the optimal number of backbone bonds to consider in the calculation of the local energy does depend on the chemical structure and that this parameter, typically equal to four[45,46,48] or five,[46] has to be optimized depending on the chemical structure of the molecule under study. Despite these reservations, the excellent agreement obtained between single-chain-sampled and MD-relaxed configurations prove that the PMC/MD generation technique, once tested on short-chain oligomers, can be used to reliably

sample the configurational phase-space of molecules of arbitrary length in the bulk melt phase.

The hybrid PMC/MD method for single-chain sampling has been described in detail elsewhere,[48] and we will only outline here its main features as applied to our copolyimides. Each 40 (dianhydride−diamine) monomer chain was independently subjected to a single-chain PMC/MD sampling procedure at 700 K, since the experimental glass-transition temperatures in these copolyimides were found to be as high as 650 K.[27] Each PMC/MD simulation was carried out for typically 150 ps with a period of 100 MD time-steps of 1 fs between attempted PMC moves.[49] Torsions within rings were excluded from the PMC sampling as they are interdependent. All other torsions were sampled irrespective of whether they are significant or not regarding the global configurations of the chain. As previous tests carried out on short polyimide oligomers had shown that the optimal number of bonds to consider in the local energy approximation is four,[48] this value was retained for the work here. The local energy difference following a pivot move was then calculated and submitted to a standard Metropolis acceptance criteria.[50] Irrespective of whether the new configuration of the chain resulting from the PMC move was accepted or rejected, there then followed 100 MD steps before the next attempted pivot. The extent of configurational decorrelation for a given chain was monitored by following the normalized autocorrelation function for its square end-to-end distance as a function of time. Configurational decorrelation for a chain typically took 20−50 ps using the PMC/MD hybrid procedure.

Three uncorrelated chains for a given system were then randomly reoriented and distributed in a periodic cubic MD box corresponding to their experimental density.[27] The respective simulation boxes thus contained a total number of atoms of 6225 for ODA-0, 6153 for ODA-20, 5865 for ODA-100, 6522 for CF_3ODA-20, and 6645 for MeOODA-20. To avoid the problem of unphysical trapping of bonds in the rings upon introduction of the excluded volume, "phantom atoms", with the mass of a carbon, were introduced upon completion of the generation procedure at the center of each cyclic group. These phantom atoms were connected to their corresponding ring atoms through flexible bonds with a force constant of 300 kg s^{-2}. This value was found to be sufficiently high to keep them close to the center of their respective rings despite the rather large initial overlap forces.

Short constant-volume molecular dynamics simulations were performed with the bending, torsions, out-of-planes and constraints switched on, while the van der Waals potential was introduced gradually. Periodic boundary conditions were applied in all three dimensions. The van der Waals potential was progressively scaled by a factor varying from 0 to 1 with a short truncation radius over a period of typically 10 ps. Velocities were rescaled at each time step to compensate for the large amount of heat produced in the system. The presence of phantom atoms and the gradual introduction of the potential led to the progressive reduction of all high energy overlaps while avoiding the unphysical entrapments. Phantom atoms were then removed and electrostatic interactions were switched on.

The simulation continued under constant-volume (NVT) conditions at 700 K for about 100−200 ps in order to further relax local hot-spots and to allow the system to come to thermal equilibrium. The temperature was maintained at a given value by loose-coupling to a heat bath[51] with a coupling constant of 0.1 ps. The system was then progressively cooled toward its target temperature of 300 K at a rate of -1 K ps^{-1}. It was switched to NPT conditions, in which the on-diagonal and off-diagonal components of the pressure tensor are maintained at ∼1 and ∼0 bar, respectively, by loose-coupling with a coupling constant of 5 ps;[52] i.e., the simulation box is allowed to relax toward its equilibrium shape and density. To further assess the extent of relaxation, an additional high-pressure (10 000 bar) and high-temperature (1000 K) NVT annealing procedure was carried out for typically 200 ps and the system was once again allowed to relax toward its equilibrium state at 300 K. In all cases, the resulting average relaxed densities were not found to change by more than 0.02 g cm^{-3}, thus confirming the efficiency of our initial procedure.

2.4. Production Runs. The simulations were run at ∼300 K until the density settled around a constant value, which typically happened after about 500 ps. The criterion for equilibration was that of Suter and coworkers in their work on hydrated polyamides[53], and bisphenol A−polycarbonate and poly(vinyl alcohol),[54] i.e. the absence of any drifts in density larger than 3×10^{-4} g cm^{-3} ps^{-1} during the last 100 ps of the equilibration procedure. This is consistent with systems in the glassy state and allows for equilibration of the systems in their local minima.[53]

A given simulation box was decomposed by the parallel code into $2 \times 2 \times 2 = 8$ domains each of ∼20 Å side length and each containing two link-cells per dimension with a length greater than the cutoff plus the shell width (1.5 Å) used in the creation of the neighbor table. Within the restriction on the cutoff and acceptable CPU costs,[55] the optimal convergence of the Ewald sum was obtained using $\alpha = 0.30$ $Å^{-1}$ and $K_{max} = 12$, while the real-space potential was truncated at 8.5 Å. The van der Waals potentials were also truncated at 8.5 Å, and long-range corrections to the energy and the pressure were calculated on the basis of the radial distribution functions being equal to unity beyond the cutoff.

Production runs were carried out for 1000 ps for each system under study, during which configurations were stored at 5 ps intervals, and thermodynamic and conformational data every 0.5 ps for post-analysis. A schematic representation of the CF_3ODA-20 system is given in Figure 2.

3. Results and Discussion

3.1. Evaluation of the Packing Models. Experimental glass-transition temperatures for the systems under study are all over 500 K.[27] When cooled to 300 K, the simulated systems also settle into an arrested state showing little overall mobility afterward, i.e., typical of the glassy state.[56] This does not prevent mobility on a local range, but as has been found in other simulations of glassy polymers,[53,54,57] the state for each system is clearly a nonequilibrium one.

To assess how strongly the results are correlated with the specific configuration of the packing model, the full preparation procedure was repeated eight times for an ODA-0 system. The eight independent simulation boxes used in this test contained two chains instead of three, i.e., 4150 atoms in order to limit the amount of necessary computational resources. The criterion for equili-

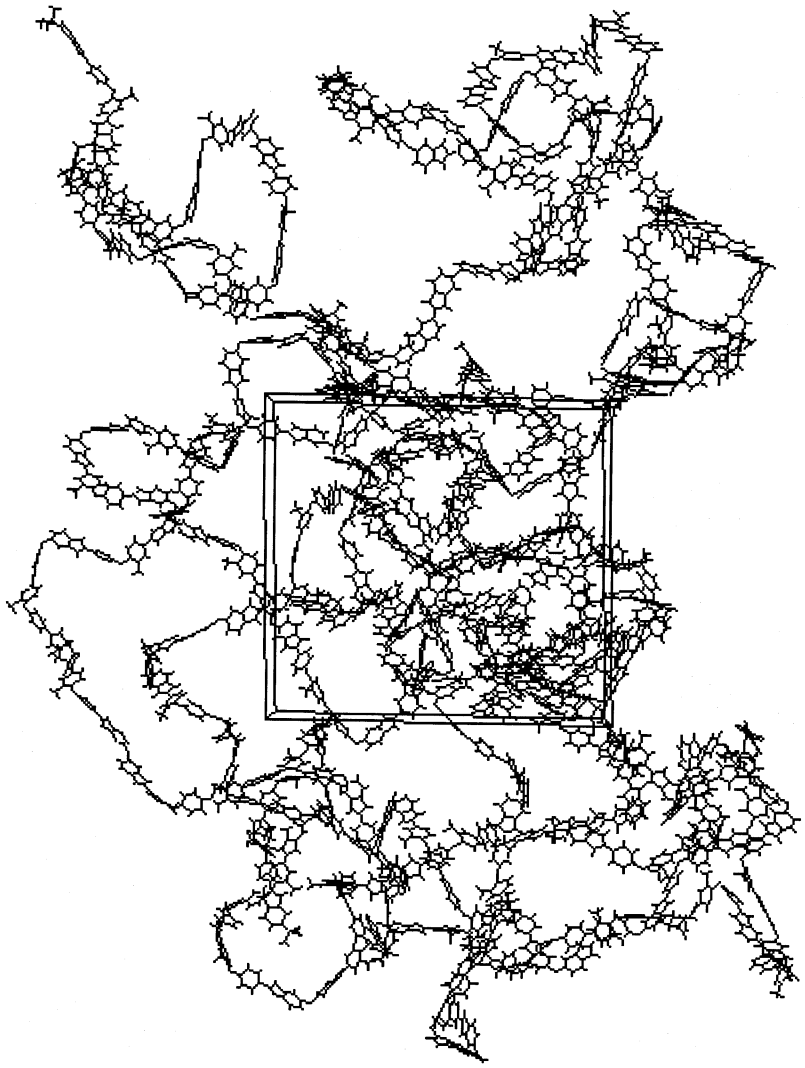

Figure 2. Schematic representation of the CF_3ODA-20 simulation box. Chains are shown in their continuous representation. The periodic boundary conditions employed ensure that all the space is filled with polymer.

Table 1. Average Relaxed Densities $\langle\rho\rangle$ in g cm^{-3} and Nearest-Neighbor Intermolecular Distances, $r_{0.5}$, Defined as $g_{inter}(r_{0.5}) = 0.5$, at 300 K for Eight Independently Prepared ODA-0 Packing Models[a]

system	$\langle\rho\rangle$/g cm^{-3}	$r_{0.5}$/Å
(ODA-0)-1	1.348	3.20
(ODA-0)-2	1.395	3.10
(ODA-0)-3	1.368	3.10
(ODA-0)-4	1.345	3.25
(ODA-0)-5	1.360	3.25
(ODA-0)-6	1.368	3.20
(ODA-0)-7	1.343	3.30
(ODA-0)-8	1.355	3.15

[a] The standard error on $\langle\rho\rangle$ is ±0.001 g cm^{-3}, and the experimental value is 1.368 g cm^{-3}. The standard error on $r_{0.5}$ is ±0.05 Å.

bration[53,54] was checked for each specific structure and the production run was 300 ps at 300 K. All other simulation details were the same as reported above.

Table 1 gives the average relaxed densities $\langle\rho\rangle$ at 300 K for the eight different ODA-0 packing models. In addition, the average indiscriminate intermolecular radial distribution functions,[9] $g_{inter}(r)$, for the ODA-0 chains were also extracted. This allowed us to compare the average nearest-neighbor intermolecular distance, $r_{0.5}$, arbitrarily defined as $g_{inter}(r_{0.5}) = 0.5$, which is quoted for each packing model in Table 1.

It is clear from Table 1 that the densities obtained for the ODA-0 models are very close to the experimentally determined value of 1.368 g cm^{-3}.[27] Indeed, they all lie within less than 2% of the experimental value, with four packing models even coming up to less than 1% of the expected density. In the literature, it is generally accepted that a difference of less than 5% can still be acceptable.[13] In their extensive work about polyimides, Hofmann et al. have used the 2% limit between simulated and experimental values as a maximum criteria to assess whether their extensive equilibration procedure for polyimide packing models was complete.[19] It is worth mentioning that although the packing procedure is quite different from ours, with insertions of small molecules to form obstacles and prevent catenation and spearing, as well as a series of high-pressure and high-temperature annealing steps which are outlined in refs 20 and 58, the aim is the same, i.e., to get model densities which are as close as possible to the experimental values. In this work, the similar order of agreement obtained between simulated and experimental densities for our ODA-0 systems thus suggests that our procedure for creating packing models of polyimides in the glassy state is both adequate and repeatable. In addition, it is also a strong validation for the force-field used in the case of ODA-0.

Table 2. Results of the MD Simulations Undertaken at 300 K for the Five Systems under Study[a]

properties	ODA-0	ODA-20	ODA-100	CF_3ODA-20	MeOODA-20
$\langle\rho\rangle_{simul}$	1.377	1.349	1.297	1.417	1.373
$\langle\rho\rangle_{exp}$	1.368	1.361	1.326	1.423	
$\langle V\rangle$	70 750	70 350	65 600	76 800	73 600
$\langle U_{pot}^{inter}\rangle$	−6367	−5927	−4719	−5683	−6278
$\langle U_{LJ}^{inter}\rangle$	−5669	−5203	−3951	−5184	−5511
$\langle U_{coul}^{inter}\rangle$	−698	−724	−768	−499	−767
δ	21.17	20.48	18.93	19.20	20.61

[a] The average relaxed model densities $\langle\rho\rangle_{simul}$ and the experimental densities $\langle\rho\rangle_{exp}$ measured in *m*-cresol are given in g cm^{-3} with a maximum standard error of ± 0.001 g cm^{-3}. The experimental density for the MeOODA20 system is not available. $\langle V\rangle$ are the average volumes of the MD cells in Å^3 with a maximum standard error of ± 50 Å^3. The average potential intermolecular energies $\langle U_{pot}^{inter}\rangle$ as well as their resolution into van der Waals $\langle U_{LJ}^{inter}\rangle$ and Coulombic $\langle U_{coul}^{inter}\rangle$ terms are quoted in kJ mol^{-1} molecule^{-1} with a maximum standard error of ±5 kJ mol^{-1} molecule^{-1}. The Hildebrand solubility parameter, δ, is given in (J cm^{-3})$^{1/2}$ with a standard error of ±0.02 (J cm^{-3})$^{1/2}$.

Experimentally determined *d*-spacings, as obtained using wide-angle X-ray diffraction,[27] are commonly thought to represent the mean interchain distances in a system[59] and thus can be compared to the average nearest-neighbor intermolecular distances. The $r_{0.5}$ for the eight independent samples all fall within the range 3.1−3.3 Å. This confirms that the models prepared using the procedure described in section 2 are quite consistent. The specific configuration of the packing model used for a given system should thus have a limited influence on the results.

3.2. Bulk Properties. The average relaxed densities $\langle\rho\rangle$ of the five systems under study (ODA-0, ODA-20, ODA-100, CF_3ODA-20, and MeOODA-20; see Figure 1) are given at 300 K in Table 2, along with the average volumes $\langle V\rangle$ of the MD cells. Also shown in Table 2 are the average intermolecular potential energies, $\langle U_{pot}^{inter}\rangle$, plus their resolution into van der Waals and Coulombic contributions, and the Hildebrand solubility parameter, δ, defined as

$$\delta = \sqrt{\frac{\langle U_{pot}^{inter}\rangle}{\langle V\rangle}} \qquad (7)$$

3.2.1. Density. The average model densities $\langle\rho\rangle_{simul}$ are all found to be close to the corresponding experimental densities $\langle\rho\rangle_{exp}$.[27] Indeed, the difference between simulated and experimental values is 0.7% for ODA-0, 0.9% for ODA-20, 2.2% for ODA-100, and 0.4% for CF_3-ODA-20. It is interesting to note that the discrepancy between simulated and experimental densities seems to increase with the BCDA content. This might be related to the exclusive choice of the lowest-energy boat−boat isomer of the BCDA fragment, whereas there is a strong possibility that higher-energy boat−chair and chair−chair isomers also exist in the real systems. However, as was pointed out before, we do not have any experimental evidence available concerning the proportions of the different isomeric forms. Another point to reflect upon is that experimental systems are also dependent on external factors such as the solvent used for processing the films[27] or the ambiant environmental conditions.[60] In addition, three simulated densities out of four differ with less than 1% from their corresponding experimental values and even the ODA-100 system falls well within the 5% limit mentioned above. As far as MeOODA-20 is concerned, the experimental density is not available but the model density also falls within the expected range for polyimides.

As is seen experimentally, the density is found to decrease with the BCDA content. This trend can be related to the steric hindrance brought about by this bulky motive. The addition of a trifluoromethyl group on the diamine leads to the highest-density system, which is also in agreement with experiment. However, Table 2 shows that the CF_3ODA-20 model also has the largest molar volume, and the increase in density is thus related to the overcompensation of the volume expansion by the extra mass associated with the fluorine groups. On the other hand, the MeOODA-20 model suggests that replacing the trifluoromethyl with a methoxy group would have a more limited effect on the density of the unsubstituted copolyimide as the smaller increase in volume is slightly overcompensated by the increase in mass.

3.2.2. Energy. Consistent with the densities, average intermolecular potential energies $\langle U_{pot}^{inter}\rangle$ tend to increase with the BCDA content, thus indicating that the systems are less tightly packed. This agrees with experimental *d*-spacings obtained using wide-angle X-ray diffraction.[27] $\langle U_{pot}^{inter}\rangle$ are mostly dominated by van der Waals $\langle U_{LJ}^{inter}\rangle$ interactions, which amount to 80−90% of the total cohesive energies. Indeed, the variations in $\langle U_{pot}^{inter}\rangle$ and $\langle U_{LJ}^{inter}\rangle$ energies are quasi-linear. On the other hand, the average Coulombic $\langle U_{coul}^{inter}\rangle$ energies have a tendency to slightly reinforce cohesion with increasing BCDA content. However, the dominating factor in these energetic terms is undoubtedly the steric effect brought about by the BCDA moiety.

While the volume of the CF_3ODA-20 simulation box is ∼9.2% larger than that of the unsubstituted copolyimide, the addition of a trifluoromethyl group on the diamine only leads to a 4% decrease in packing energy. This is due to two main antagonistic factors, i.e., the steric repulsion brought about by the presence of a trifluoromethyl group (with a van der Waals volume of 21.3 vs 3.4 cm^3 mol^{-1} for a hydrogen[61]) and the attractive interactions due to the partial charges carried by the fluorine atoms ($q/e \simeq 0.15$). As a result, the overall decrease in cohesion exhibited by the intermolecular energies remains relatively limited with respect to the change in volume. On the other hand, the volume expansion following the addition of a smaller methoxy group (with a van der Waals volume of 17.4 cm^3 mol^{-1} [61]) is only ∼4.5%, and the main effect on the intermolecular energy is a cohesive increase in $\langle U_{LJ}^{inter}\rangle$. The added interactions with the methoxy group thus outweigh the change in volume and its effect on the energy is opposite to that brought about by the introduction of CF_3.

3.2.3. Hildebrand Parameters. As shown by eq 7, the Hildebrand parameters are directly linked to the cohesive energy density of the different systems. They all lie well within the empirical range of $\delta = 14-28$ (J cm^{-3})$^{1/2}$, reported for polymers.[61] As expected from the densities and the total intermolecular potential energies, the cohesive energy density is inversely proportional to the amount of the BCDA moiety in the copolyimides. In a similar vein, the volume expansion effect of the trifluoromethyl group is reflected by the decrease of the cohesive energy density in the CF_3ODA-20 system. On the other hand, the overcompensation of the volume expansion by the van der Waals attractions

in the MeOODA-20 model are shown in the slight increase of the cohesive energy density with respect to the unsubstituted system. It is interesting to note that the solubility parameter could thus be fine-tuned in these types of systems depending on the choice of substituent. The problem of limited solubility is indeed a major one in the field of polyimides.[1]

These parameters can also be empirically estimated through the group contribution approach.[61] Values obtained for the polyimides under study fall within the 25−32 $(J\ cm^{-3})^{1/2}$ range[62,63] and are thus higher than the simulated δ. However, these empirical parameters do not reproduce the experimental solubilities of the copolyimides under study in various solvents.[27] In addition, the empirical Hildebrand parameters evaluated using the Hoy method[62] vary in the order δ(ODA-20) < δ(CF_3ODA-20), while δ(ODA-20) > δ(CF_3ODA-20) using the Fedors method.[63] These shortcomings have been linked to the inability of the group contribution approach to take into account the isomeric structures of the rings as well as the lack of parameters for some functional groups.[27] The empirical Hildebrand parameters can thus not really be used as a validation for our models. However, it should be mentioned that the decrease in δ as the BCDA content increases, i.e., δ(ODA-0) > δ(ODA-20) > δ(ODA-100), is found both using the Hoy[62] and the Fedors[63] methods,[27] and is consistent with the values shown in Table 2.

Another way to validate the quality of such models is the calculation of solubilities for small gas molecules, as has been done for other polyimide systems.[18−20,64] Solubility coefficients can be obtained using the particle insertion technique of Widom.[65,66] Such calculations have been carried out on all five models with He, O_2, and N_2 molecules and the results were found to be of the same orders of magnitude than those reported in refs 18−20 and 64. However, as we do not have at present any direct experimental data available with which to compare them, we intend to report on these aspects at a later stage.

3.3. Structural Properties. 3.3.1. Indiscriminate Intermolecular Radial Distribution Functions. As described in other simulation works,[12,13] the indiscriminate intermolecular radial distribution functions for the chains, $g_{inter}(r)$, can be used to assess whether the atomistic model systems are really amorphous or whether they exhibit some crystalline characteristics. Experimentally, all the copolyimides were found to be fully amorphous using X-ray diffraction analyses with the exception of the ODA-0 film which had a crystallinity ratio of about 10%.[27]

The $g_{inter}(r)$, calculated over all atoms in a given system are shown in Figure 3. They reveal no apparent order and all five models can thus be considered as amorphous. Global intermolecular radial distribution functions were also analyzed for polyimide backbone atoms, i.e., only ring atoms were taken into account. These $g_{inter-backbone}(r)$ functions are very similar to the corresponding $g_{inter}(r)$ and remain in the same relative order.

The $r_{0.5}$, which reflect the interchain distances in the systems, are found to increase in the order ODA-0 < ODA-20 ≈ MeOODA-20 < CF_3ODA-20 < ODA-100. Results are consistent with the evolution of the experimental *d*-spacings as a function of the percentage of BCDA, which were estimated to be 4.7 Å for ODA-0, 5.3 Å for ODA-20 and 5.4 Å for ODA-100 in the reflection mode. The corresponding experimental *d*-spacings obtained in the transmission mode are 4.5 Å for ODA-0, 5.0 Å for ODA-20 and 5.6 Å for ODA-100.[27] Although the *d*-spacing is defined by the position of the maximum in the amorphous halo in X-ray diffractograms, and as such can be rather ill-defined, it does follow the general trend of larger interchain distances as the BCDA content increases. Experimental *d*-spacings for the CF_3ODA-20 system were estimated in the reflection mode at 5.0 Å in *m*-cresol,[27] i.e., the same order of magnitude than the ODA-20 system. Our models suggest that interchain distances remain similar upon adding a methoxy group while, as is the case with BCDA, they slightly decrease with trifluoromethyl substituents in agreement with the energy analyses.

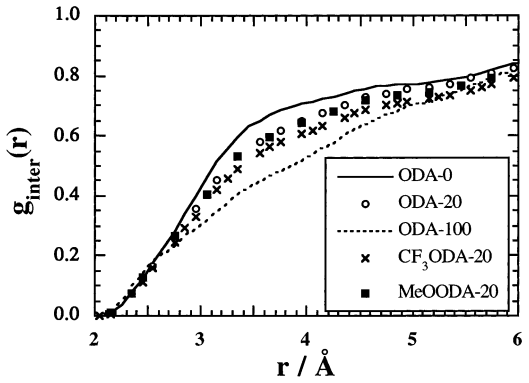

Figure 3. Indiscriminate intermolecular radial distributions averaged over all atom pairs and over all configurations for each system under study.

3.3.2. Conformational Analyses. The large number of rings in the stiff polyimide backbones means that the only real conformational backbone degrees of freedom are the so-called "pivot angles", i.e., rotations around the nitrogen−phenyl bonds of the dianhydride−diamine linkages (C−N−C−C torsions) and around the ether linkages of the diamine and ODPA moieties (C−O−C−C torsions) (see Figure 1).

In the TRIPOS 5.2 force-field,[31] the bending equilibrium angles are set to 120° for the C−N−C dianhydride−diamine linkages and to 110° for the C−O−C ether bridges. In all cases, the steric and electronic repulsions between the rings leads to the opening of the angles. Indeed, the average values for C−N−C angles are ∼126.0° for all ODPA−ODA and ∼124.2° for all BCDA−ODA fragments. This offset can be linked to the imide oxygen/ODA hydrogen electrostatic interactions which are more attractive in the BCDA−ODA monomer. The C−O−C bends in the ODPA and ODA fragments are more flexible and their average values fall in the 114.8−117.5° range, the differences being related to the distributions of C−C−O−C dihedral angles.

The underlying probability density distributions for the pivot dihedral angles are shown in Figure 4 in the case of the ODA-0 model. N.B. in the convention used here, the dihedral angle varies from −180 to +180° with τ = 0° corresponding to the trans conformation, i.e., where all four atoms lie in the same plane and atoms at either end are at their furthest distance apart. The dianhydride−diamine ODPA−ODA distributions exhibit four well-defined peaks located at around ±30° and ±150°, which correspond to the four possible C−C−N−C angles around a linkage. The corresponding BCDA−ODA distributions (not shown) are very similar.

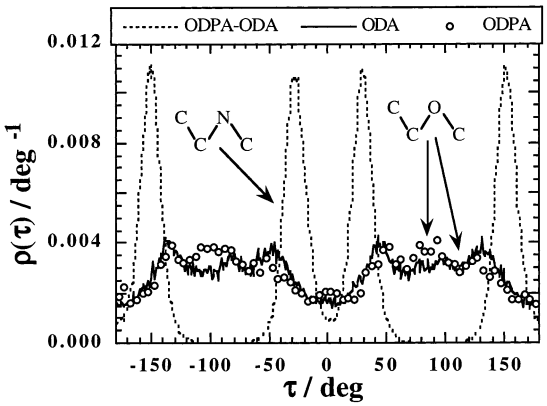

Figure 4. Compared dihedral angles probability densities for the ODPA−ODA C−C−N−C dihedral angles as well as the ODA and the ODPA C−C−O−C ether bridges in the ODA-0 model.

The rotational barriers are much lower in the case of the ODA and ODPA ether linkages. Figure 4 shows that there are no clear peaks centered around specific values and that they actually span the whole domain of possible torsion angles. The H···H interactions on either side of the rings cause the C−C−O−C dihedrals to have a small preference for gauche conformations, which is also slightly enhanced by either trifluoromethyl or methoxy substituents. However, the high flexibilities of these ether bridges is maintained in all five systems under study and their C−C−O−C distributions are very similar. It should be mentioned that differences in the conformational behavior could not be either clearly distinguished in a recent comparative study of BCDA−ODA and PMDA−ODA (PMDA = pyromellitic dianhydride) oligomers.[67] This would suggest that the pivot angles are thus only governed by very local intramolecular factors which are common to all these polyimides, i.e., the dianhydride imides and the aromatic rings.

The C−C−C−F dihedrals in the CF_3ODA-20 model span the whole domain of possible torsion angles, which is characteristic of very freely rotating groups. Indeed, the trifluoromethyl group is symmetric and fairly spheric with respect to rotations around the central bond of the C−C−C−F torsions. The distributions for the C−C−O−CH_3 dihedral angles in the MeOODA-20 model are more structured, so rotations in this case are likely to be more restricted. This is related to the asymmetry of the methoxy group which implies a significant rearrangement of the local structure to allow rotations around the central bond of the C−C−O−CH_3 torsions. The added cohesive terms in the intermolecular energy of the MeOODA-20 model (see Table 2) will further enhance these restrictions.

3.3.3. Specific Intermolecular Radial Distribution Functions. To determine whether the different copolyimides exhibit preferential structural arrangements between dianhydride and/or diamine fragments, specific intermolecular radial distribution functions $g_{A\cdots B}(r)$ were calculated from the positions of the atoms belonging to the six-atom ring moieties of the respective dianhydrides and the two phenyl rings of the diamines. These $g_{A\cdots B}(r)$ were integrated to give the total number of atoms belonging to ring B within a radius r of an atom belonging to ring A

$$n_{A\cdots B}(r) = 4\pi \frac{N_B}{\langle V \rangle} \int_0^r g_{A\cdots B}(s) s^2 \, ds \qquad (8)$$

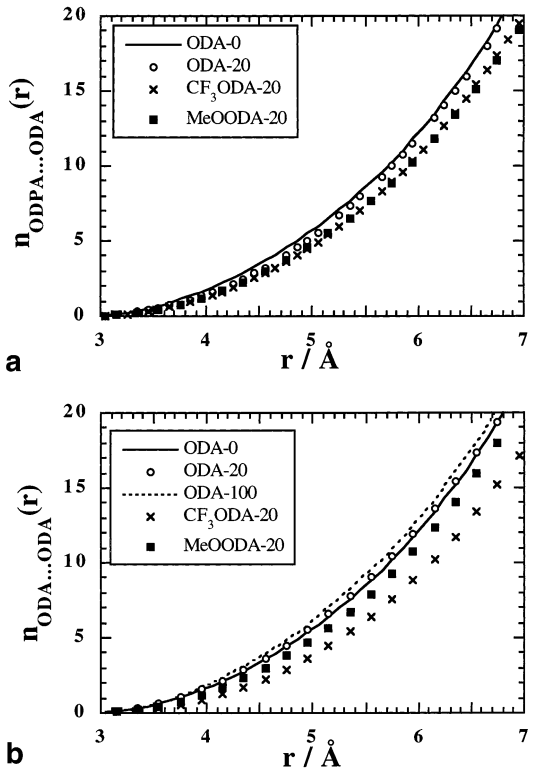

Figure 5. Intermolecular $n_{A\cdots B}(r)$ curves for (a) ODPA aromatic carbons with ODA aromatic carbons and (b) ODA aromatic carbons with themselves as a function of the chemical structure of the copolyimide.

where N_B is the total number of atoms belonging to a ring B in the system, and $\langle V \rangle$ is the average volume of the simulation box. This allows direct comparisons between models which have different $\langle V \rangle$ (Table 2). It should be mentioned that in all cases where the ODPA or the BCDA moiety was included in the analyses, the closest interactions found were those with the carbonyl oxygens of the imide groups, since these atoms are much more accessible than those in the sheltered middle parts. However, for better comparison, analyses were carried out on those parts which differ in both dianhydrides, i.e., their six-atom rings. Within a given system, the stacking of planar aromatic rings (mainly ODA−ODA and ODA−ODPA followed by ODPA−ODPA) were always the predominant interactions, as they are themselves more accessible than the bulky BCDA fragments.

$n_{A\cdots B}(r)$ are shown in Figure 5a for interactions where an ODPA aromatic ring is of type A and an ODA aromatic ring is of type B. These specific interactions are particularly relevant with regard to charge-transfer complexes (CTC),[68] which are known to occur in some polyimides.[4,69−73] These CTC form by electron transfer between electron-rich diamine rings and electron-deficient dianhydride rings and have been characterized by UV spectroscopy,[4] solid-state ^{13}C NMR,[70] ^{15}C NMR,[71] and fluorescence spectroscopy.[72,73] Although classical molecular dynamics simulations do not allow for electron transfer, it is obvious that direct orbital interactions are only possible if both moieties come into close contact.[71] UV spectrophotometry analyses show that ODA-0 and ODA-20 have very similar color indices which are higher than that of CF_3ODA-20.[27] Such high color indices have been directly linked to the formation of the CTC in the literature.[68]

It should also be pointed out that for other aromatic molecules,[74,75] both the inter-ring distance *and* the extent of overlap of the aromatic system were found to contribute to the color. Although we do not explicitly calculate overlap integrals, we note that the $n_{A\cdots B}(r)$ curves implicitly include information on both distances and overlaps as they are averaged over all possible interatom distances between the rings; two aromatic rings perfectly stacked on top of each other will give rise to the largest number of short distances.

Figure 5a shows that the simulation data is consistent with experiment where ODPA−ODA interactions are less predominant when the diamine is substituted; whether it be by a trifluoromethyl or by a methoxy group. Shorter distances and maximum overlap are found in the systems which stack easier, i.e., ODA-0 and ODA-20. On the other hand, the $n_{BCDA\cdots ODA}(r)$ curves are rather similar in all three ODA-20, CF_3ODA-20, and MeOODA-20 systems. These interactions are thus almost totally dominated by the dissymmetric space-filling of the BCDA dianhydride, which prevents easy stacking in the first place. Indeed, the experimental color indices are found to decrease as the percentage of BCDA increases.[27] In addition, its middle ring is alicyclic and nonaromatic. Adding BCDA moieties or substituents on the diamine will thus in all cases lower the possibilities of CTC formation, which are known to restrict the available space within polyimide matrixes.[1−3]

Diamine−diamine $n_{ODA\cdots ODA}(r)$ are shown in Figure 5b. While they are rather similar for the unsubstituted systems (with a slightly favored interaction in the ODA-100 related to the lack of competition for stacking with the dianhydride), they differ in the ODA-20 based models. The main effect is due to the polar trifluoromethyl group which leads to significant repulsions between the ODA rings and pushes the chains apart. On the other hand, the smaller and less repulsive methoxy substituent will not shift too much the $n_{ODA\cdots ODA}(r)$ curves with respect to the unsubstituted system. The same phenomenon can be seen on the dianhydride-dianhydride $n(r)$, where the methoxy copolyimide always has an intermediate behavior between the unsubstituted and the trifluoromethyl copolyimide.

To further assess the structural interactions associated with the substituents on the diamine, intermolecular $n_{A\cdots B}(r)$ with A being different atom types and B being either fluorine atoms or methoxy hydrogens, were also examined. The closest interactions found are always with the ketone oxygens on the dianhydrides, and in most cases, both types of substituents behave in the same way except that the interactions with fluorine are slightly shifted toward larger distances. This is related to the larger steric and electronic repulsion of a fluorine with respect to a hydrogen and suggests that none of the substituents seem to form a particularly favored interaction with a specific site on the copolyimide. Although both the trifluoromethyl and the methoxy group will affect the void space, their influence on the polyimide conformations remains very limited as suggested by the conformational analyses. This conclusion is further supported by a separate series of hybrid PMC/MD single-chain sampling 5 ns runs (results not displayed), where the distributions of average square end-to-end distances and average square radii of gyrations are found to be quite similar for the unsubstituted and substituted copolyimides.

3.4. Morphology of the Void Space. To complement the other analyses, the amount of "void space" and the manner in which it is distributed were characterized. There have been many attempts to estimate the morphology of void space using for example empirical calculations,[61,76] positron annihilation experiments,[7,8] labeling and probes,[77] or atomistic simulations.[58,78−80]

Within this framework, we used a method based on the "phantom sphere approach",[78,79] which is similar to that described in a recent paper by Hofmann et al.[58] In their work, the authors lay a three-dimensional grid over the simulation boxes and test at each grid point whether a hard sphere with a given volume overlaps hard spheres representing the polymer atoms.[58] In our approach, the accessible space is instead obtained by a Monte Carlo procedure in which probes of a preset radius are randomly and independently inserted into the MD configurations previously stored. The polymer atoms are represented by hard spheres with standard van der Waals radii, i.e., 1.20 Å for H, 1.47 Å for F, 1.50 Å for O, 1.55 Å for N, and 1.70 Å for C.[61,76] Five million trial insertions are attempted for each system, and only those probes which do not overlap with the copolyimide atom hard spheres are accepted. The percentage of probe-accessible volume (% PAV) is then simply the percentage of accepted insertions. The probe-accessible volume itself (PAV) is the product of the probability of accepting an insertion with the volume of the simulation box. To further characterize the PAV distribution, the positions of all accepted probes are stored and distances between them are subjected to an interaction limit R_p which links those probes having been inserted into the same "hole" for a given configuration. The subsequent "clusters" of linked probes can then be used to define the volumes of the individual holes from the proportion of the total number of accepted probes in the holes and the total PAV of the configuration. This is also very similar to the "V_connect" approach of Hofmann et al.,[58] where the neighboring "free" grid points are put together in the same groups. However, it is obvious that the resulting distributions will depend very much on the choice of R_p. For example, small values of R_p lead to distributions where each probe forms its own separate hole whereas large values of R_p give just one large percolating cluster. By trial and error, a value of $R_p = 0.65$ Å for a probe of radii 1.1 Å (i.e., corresponding to the size of a positronium) was found to lead to distributions with a range of hole sizes that could be used to compare the different systems in a relative way. This value is also similar to the grid lattice spacing of ref 58, i.e., 0.7 Å. All results were averaged over all the stored configurations for a given system.

It should be stressed that this analysis gives only access to global free volume regions and does not as yet lead to any real information about the shape of the holes. Other techniques have been proposed in order to better exploit information from MD simulations and to compare, for example, with positron annihilation lifetime spectroscopy (PALS). One is the "R_max" approach of Hofmann et al.,[58] which in a further step from the "V_connect" mentioned above, finds local maxima of shortest distances among the "free" grid-points, and decomposes complex holes into more local regions. Another one is that of Schmitz and Müller-Plathe,[80] who have designed a path integral Monte Carlo method to directly calculate the positronium lifetime in the free volume sites in order to extract spectra and free volume

Table 3. Average Percentages of Probe-Accessible Volume (% PAV) in the Different Systems as a Function of the Probe Radius[a]

probe radius/Å	ODA-0	ODA-20	ODA-100	CF_3ODA-20	MeOODA-20
0	34.17	35.29	37.25	35.89	33.97
0.4	13.56	14.17	15.99	15.13	12.63
0.6	7.70	8.02	9.40	8.97	6.72
0.8	4.11	4.25	5.15	5.06	3.28
0.9	2.94	3.02	3.71	3.72	2.22
1.0	2.08	2.12	2.61	2.71	1.47
1.1	1.45	1.47	1.80	1.94	0.95
1.2	1.00	1.00	1.21	1.37	0.61
1.3	0.69	0.67	0.80	0.95	0.38
empirical FFV	13.4	13.6	14.9	16.4	

[a] Errors in the % PAV are ±1 in the last figure quoted. The experimental FFV (free volume fractions) are empirically estimated from the real densities using the Bondi method.[61,76]

properties. However, we do not have as yet available PALS results on the copolyimides under study to compare with and so this is beyond the scope of the paper. Instead, we attempt a global comparison of the void-space morphology by applying the same basic assumptions to our selection of copolyimides.

The % PAV are given in Table 3 for probe radii ranging from 0 to 1.3 Å. Also shown in Table 3 are the free volume fractions (FFV) empirically estimated from the experimental densities using the Bondi method.[61,76] Although this approach is known to be rather approximate mainly because of the consideration of a universal scaling factor of 1.3 for the van der Waals volumes in the estimation of the occupied volume, the various corrections for intramolecular crowding and association bonding[81] and the approximation of spheric geometries for whole groups of atoms,[61,76] the empirical values reported in Table 3 fall well within the usual range of FFV for polyimides, i.e., from 10 to 20.[82,83] In our approach, the closest values to the Bondi FFV are obtained using a probe size of 0.4 Å. The same conclusion was reached by Hofmann et al.[58] in their work on PTMSP, PTMSS, and PFDMSS polymers, where the best agreement between Bondi and simulated FFV was found for a probe size of 0.43 Å. As expected, smaller probe sizes lead to higher values, with the zero radius probe representing the total free volume, i.e., the total volume not occupied by the polymer atoms. However, a zero radius probe will sample volume which can never be accessed and results should be more meaningful for probes eliminating this artifact, such as the positronium 1.1 Å probe. In addition, information can be obtained from the variation of the % PAV with the probe size which will be characteristic for a given polymer.

With small probes (up to 0.8 Å), the relative order of the % PAV was consistently MeOODA-20 < ODA-0 < ODA-20 < CF_3ODA-20 < ODA-100. The order remained the same for larger probes, except that the CF_3ODA-20 was found to have a larger % PAV than the ODA-100, which is consistent with the experimental FFV. The void space is thus found to increase along with the introduction of the BCDA dianhydride as this fragment leads to larger interchain distances. In addition, its geometry with the bridge on one side is asymmetric and small probes will be accepted inside the space already occupied by the BCDA moiety. However, the system exhibiting the highest % PAV for probes over 0.9 Å is the CF_3ODA-20 model. This is consistent with the literature on fluorine substituents, where their steric and electronic

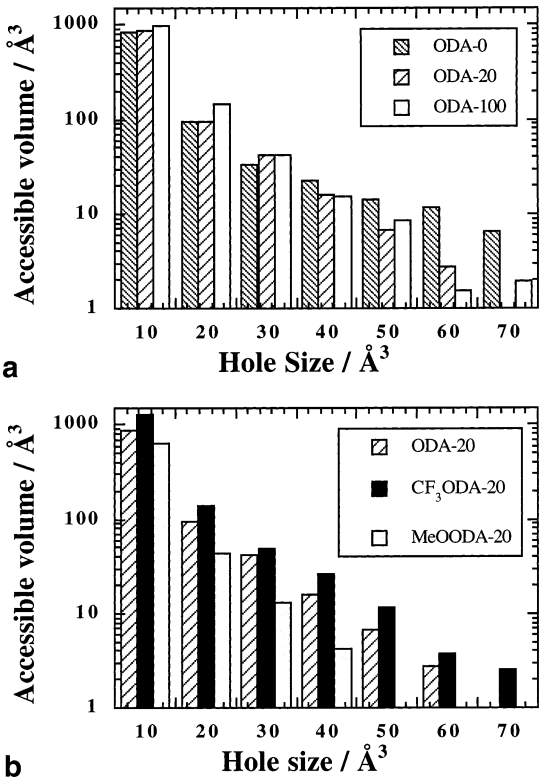

Figure 6. Distributions of the amount of volume accessible to trial insertions of a 1.1 Å radius probe with an interaction parameter of $R_p = 0.65$ Å as a function of the hole size: (a) distributions for the ODA-0, ODA-20, and ODA-100 models (b) distributions for the ODA-20, CF_3ODA-20, and MeOODA-20 models.

repulsive effects are considered quite efficient in keeping the polymer chains apart.[84−87] On the other hand, the MeOODA-20 exhibits the smallest amount of void space despite a larger simulation box than all the unsubstituted polyimides (cf. Table 2). The methoxy groups thus have a tendency to occupy a part of the void space which already exists in the unsubstituted systems. This is consistent with the relatively similar interchain distance (see Figure 3) in both ODA-20 and MeOODA-20 models and the limited swelling of the MeOODA-20 simulation box.

The underlying PAV distributions for the 1.1 Å probe, corresponding to the positronium radius, and an $R_p = 0.65$ Å are shown in Figure 6. Figure 6a compares the three unsubstituted systems, i.e., ODA-0, ODA-20, and ODA-100. The smallest and largest amount of small holes (accessible volume less than 10 Å^3) are found in the ODA-0 and ODA-100 homopolyimides, respectively. These are obviously largely related to the planar aromatic-ring-based geometry of the ODPA dianhydride while the BCDA dianhydride has a kinked and bulky geometry. The flexible ODPA-based system (ODA-0) will thus lead to an extended distribution which is characterized by more accessible volume in the form of larger hole sizes. The rigid BCDA-based system (ODA-100) favors voids in the small to medium range of hole sizes. This is consistent with the fact that BCDA−ODA-based oligomers were found to favor smaller holes with respect to their planar and more regular PMDA−ODA counterparts.[67] The coexistence of both types of dianhydrides on the polyimide chain (ODA-20) leads to a reorganization of the void space. Indeed, this system has an intermediate behavior between both homopolyimides

with respect to the smallest holes, but its distribution decreases faster and there are no large holes in the model.

Figure 6b examines the effect of the diamine substituent on the void morphology by comparing the ODA-20, CF_3ODA-20, and MeOODA-20 models. The trifluoromethyl substituent is found to significantly increase the whole population of voids with respect to the unsubstituted copolyimide, and even leads to a distribution which is reminiscent of the ODA-100 system (Figure 6a). The methoxy substituent has the opposite effect. It does not really lead to any new holes and even decreases the population of voids by occupying holes which are already there in the unsubstituted system.

4. Conclusions

Five MD simulations have been successfully undertaken on a series of copolyimides and the chemical influence of increasing the BCDA content and introducing a trifluoromethyl or a methoxy substituent on the ODA diamine has been studied. For four of the five systems, the results have been directly compared to previously obtained experimental data[26,27] for copolyimide chains of about the same molecular weight and sequence of monomers, although an unanswered question relates to the proportion of boat−boat, boat−chair, and chair−chair conformers for the BCDA groups; they are considered to be 100% boat−boat in the simulations but are actually unknown in the experiments. Experimental results for densities, color indices, and free-volume fractions were used to validate the models.

The initial copolyimide amorphous chain configurations were efficiently prepared using a hybrid PMC/MD-sampling technique, which had already been extensively tested elsewhere.[41,43−45,46,47,48] The reproducibility of this preparation procedure has been assessed in this work by repeating the procedure eight times for the ODA-0 model used here. The good agreement found for the average relaxed densities and indiscriminate intermolecular radial distribution functions confirmed the validity of the hybrid PMC/MD polymer sample preparation procedure.

These MD simulations demonstrate that increasing the amount of BCDA within a copolyimide system introduces much steric hindrance and, as a consequence, decreases the density, the cohesive energy and the Hildebrand solubility parameter. In addition, interchain distances are larger, charge-transfer complexes are more limited, and the amount of probe-accessible volume is higher. This should increase the diffusivity in BCDA-based systems. However, the fact that its dissymmetric bulky structure leads to more small-to-medium-range holes is a good indication toward specific selectivity.

Both diamine substituents under study were found to have very different consequences. Despite a high CF_3-ODA-20 density, the trifluoromethyl expands the simulation box and decreases the Hildebrand solubility parameter. With its symmetric freely rotating shape and its combined steric and electronic repulsions, the chains are pushed apart and charge-transfer complexes are likewise limited. Its probe-accessible volume is the highest of all and results from an increase of all holes sizes with respect to the unsubstituted copolyimide.

In contrast, the MeOODA-20 methoxy group only leads to a slight volume expansion which is compensated by added cohesive interactions. Its density, its cohesive energy density and interchain distances remain very similar to those of the ODA-20 model. The methoxy group has less mobility because of its asymmetric shape, and its steric effect is fairly limited. Its probe-accessible volume is the lowest of all systems as the methoxy groups fill holes which would exist if the copolyimide was unsubstituted.

These five systems could be distinguished in several ways at the molecular level although one exception was the conformational properties of the backbone inter-ring pivot angles. It is clear that the BCDA moiety and the trifluoromethyl substituent on the diamine have a similar qualitative effect on the properties of the copolyimides. They both increase the available void space and decrease chain cohesion, thus leading to more promising systems as far as diffusion of small molecules is concerned. This will be the subject of further investigations. On the other hand, the repulsive effect of the methoxy group is not strong enough to significantly differ from the unsubstituted system.

Acknowledgment. The IDRIS (Orsay, France) and the CINES (Montpellier, France) supercomputing centers are acknowledged for the provision of computer time, as well as local resources at the University of Savoie (COMPAQ DS20E). The Rhône-Alpes region is thanked for funds dedicated to computer hardware, and A. Fogola is thanked for helping with the preparation of repeated ODA-0 simulations.

Supporting Information Available: A series of tables containing all the partial charges used in this work (see eq 6). This material is available free of charge via the Internet at http://pubs.acs.org

References and Notes

(1) *Polyimides: Fundamentals and Applications*; Marcel Dekker: New York, 1996.
(2) Ohya, H.; Kudryavtsev, V. V.; Semenova, S. I. *Polyimide Membranes−Applications, Fabrication and Properties*; co-published by Kodansha Ltd. and Gordon and Breach Science Publishers S.A.: Tokyo and Amsterdam, 1996.
(3) *STEPI 5 Conference Proceedings, Polyimide and High Performance Polymers*; Abadie, M. J. M., Sillion, B., Eds.; LEMP/MAO: Montpellier, France, 2001.
(4) LaFemina, J. P.; Arjavalingam, G.; Houghman, G. *J. Chem. Phys.* **1989**, *90*, 5154.
(5) Kitano, Y.; Usami, I.; Obata, Y.; Okuyama, K.; Jinda, T. *Polymer* **1995**, *36*, 1123.
(6) Brillhart, M. V.; Yao Yi, C.; Nagarkar, P.; Cebe, P. *Polymer* **1997**, *38*, 3059.
(7) Tao, S. J. *J. Chem. Phys.* **1972**, *56*, 5499.
(8) Schrader, D. M.; Jean, Y. C. *Positron and Positronium Chemistry*; Elsevier: Amsterdam, 1988.
(9) Allen, M. P.; Tildesley, D. J. *Computer Simulation of Liquids*; Clarendon Press: Oxford, England, 1987.
(10) Gelin, B. R. *Molecular Modeling of Polymer Structures and Properties*; Carl Hanser Verlag: Munich, Germany, 1996.
(11) Zhang, R.; Mattice, W. L. *Macromolecules* **1993**, *26*, 6100.
(12) Zhang, R.; Mattice, W. L. *Macromolecules* **1995**, *28*, 7454.
(13) Kang, J. W.; Choi, K.; Jo, W. H.; Hsu, S. L. *Polymer* **1998**, *39*, 7079.
(14) Sundararajan, P. R.; Sacripante, G.; Wang, Z. Y. *Comput. Theor. Polym. Sci.* **2000**, *10*, 219.
(15) Smit, E.; Mulder, M. H. V.; Smolders, C. A.; Karrenbeld, H.; Van Eerden, J.; Feil, D. *J. Membr. Sci.* **1992**, *73*, 247.
(16) Zhang, R.; Mattice, W. L. *J. Membr. Sci.* **1995**, *108*, 15.
(17) Hofmann, D.; Ulbrich, J.; Fritsch, D.; Paul, D. *Polymer* **1996**, *37*, 4773.
(18) Hofmann, D.; Fritz, L.; Ulbrich, J.; Paul, D. *Comput. Theor. Polym. Sci.* **2000**, *10*, 419.
(19) Hofmann, D.; Fritz, L.; Ulbrich, J.; Schepers, C.; Böhning, M. *Macromol. Theory Simul.* **2000**, *9*, 293.

(20) Heuchel, M.; Hofmann, D. *Desalination* **2002**, *144*, 67.
(21) Yoneya, M.; Iwakabe, Y. *Liq. Cryst.* **1996**, *21*, 347.
(22) Yoneya, M.; Iwakabe, Y. *Liq. Cryst.* **1996**, *21*, 817.
(23) Van der Vegt, N. F. A.; Müller-Plathe, F.; Gelebus, A.; Johannsmann, D. *J. Chem. Phys.* **2001**, *115*, 9935.
(24) Fujiwara, I.; Ishimoto, C.; Seto, J. *J. Vac. Sci. Technol. B* **1991**, *9*, 1148.
(25) Young, J. A.; Farmer, B. L.; Hinkley, J. A. *Polymer* **1999**, 2787.
(26) Pinel, E.; Bas, C.; Neyertz, S.; Albérola, N. D.; Petiaud, R.; Mercier, R. *Polymer* **2002**, *43*, 1983.
(27) Pinel, E. Ph.D. Thesis, University of Savoie, Le Bourget-du-Lac, France, 2001.
(28) Brown, D. *the gmq user manual*, 2001. Available from http://www.univ-savoie.fr/labos/lmpc/gmq.html.
(29) Brown, D.; Minoux, H.; Maigret, B. *Comput. Phys. Commun.* **1997**, *103*, 170.
(30) *Hyperchem*; Hypercube Inc., C. H.: Gainesville, FL, (http://www.hyper.com, 1998).
(31) Clark, M.; Cramer III, R. D.; Van Opdenbosch, N. *J. Comput. Chem.* **1989**, *10*, 982.
(32) Hammonds, K. D.; Ryckaert, J.-P. *Comput. Phys. Commun.* **1991**, *62*, 336.
(33) Ewald, P. P. *Ann. Phys.* **1921**, *64*, 253.
(34) Smith, W. *Comput. Phys. Comm.* **1992**, *67*, 392.
(35) Frisch, M. J.; Trucks, G. W.; Schlegel, H. B.; Scuseria, G. E.; Robb, M. A.; Cheeseman, J. R.; Zakrzewski, V. G.; J. A. Montgomery, J.; Stratmann, R. E.; Burant, J. C.; Dapprich, S.; Millam, J. M.; Daniels, A. D.; Kudin, K. N.; Strain, M. C.; Farkas, O.; Tomasi, J.; Barone, V.; Cossi, M.; Cammi, R.; Mennucci, B.; Pomelli, C.; Adamo, C.; Clifford, S.; Ochterski, J.; Petersson, G. A.; Ayala, P. Y.; Cui, Q.; Morokuma, K.; Malick, D. K.; Rabuck, A. D.; Raghavachari, K.; Foresman, J. B.; Cioslowski, J.; Ortiz, J. V.; Baboul, A. G.; Stefanov, B. B.; Liu, G.; Liashenko, A.; Piskorz, P.; Komaromi, I.; Gomperts, R.; Martin, R. L.; Fox, D. J.; Keith, T.; Al-Laham, M. A.; Peng, C. Y.; Nanayakkara, A.; Gonzalez, C.; Challacombe, M.; Gill, P. M. W.; Johnson, B. G.; Chen, W.; Wong, M. W.; Andres, J. L.; Head-Gordon, M.; Replogle, E. S.; Pople, J. A. *Gaussian 98*; Gaussian Inc., Pittsburgh, PA, 1998.
(36) Singh, U. C.; Kollman, P. A. *J. Comput. Chem.* **1984**, *5*, 129.
(37) Fried, J. R.; Sadat-Akhavi, M.; Mark, J. E. *J. Membr. Sci.* **1998**, *149*, 115.
(38) Ferry, J. D. *Viscoelastic Properties of Polymers*, 3rd ed.; Wiley: New York, 1980.
(39) Clarke, J. H. R.; Brown, D. *Mol. Simul.* **1989**, *3*, 27.
(40) McKechnie, J. I.; Brown, D.; Clarke, J. H. R. *Macromolecules* **1992**, *25*, 1562.
(41) Brown, D.; Clarke, J. H. R.; Okuda, M.; Yamazaki, T. *J. Chem. Phys.* **1994**, *100*, 6011.
(42) Flory, P. J. *The Statistical Mechanics of Chain Molecules*; Hanser Publishers: New York, 1988.
(43) Brown, D.; Clarke, J. H. R.; Okuda, M.; Yamazaki, T. *J. Chem. Phys.* **1994**, *100*, 1684.
(44) Brown, D.; Clarke, J. H. R.; Okuda, M.; Yamazaki, T. *J. Chem. Phys.* **1996**, *104*, 2078.
(45) Neyertz, S.; Brown, D. *J. Chem. Phys.* **1995**, *102*, 9725.
(46) Neyertz, S.; Brown, D. *J. Chem. Phys.* **1996**, *104*, 10063.
(47) Neyertz, S.; Brown, D.; Clarke, J. H. R. *J. Chem. Phys.* **1996**, *105*, 2076.
(48) Neyertz, S.; Brown, D. *J. Chem. Phys.* **2001**, *115*, 708.
(49) Lal, M. *Mol. Phys.* **1969**, *17*, 57.
(50) Metropolis, N.; Rosenbluth, A. W.; Rosenbluth, M. N.; Teller, A. H.; Teller, E. *J. Chem. Phys.* **1953**, *21*, 1087.
(51) Berendsen, H. J. C.; Postma, J. P. M.; Van Gunsteren, W. F.; DiNola, A.; Haak, J. R. *J. Chem. Phys.* **1984**, *81*, 3684.
(52) Brown, D.; Clarke, J. H. R. *Comput. Phys. Comm.* **1991**, *62*, 360.
(53) Knopp, B.; Suter, U. W. *Macromolecules* **1997**, *30*, 6114.
(54) Nick, B.; Suter, U. W. *Comput. Theor. Polym. Sci.* **2001**, *11*, 49.
(55) Fincham, D. *Mol. Simul.* **1994**, *13*, 1.
(56) Sperling, L. H. *Introduction to Physical Polymer Science*; John Wiley and Sons: New York, 1986.
(57) Knopp, B.; Suter, U. W.; Gusev, A. A. *Macromolecules* **1997**, *30*, 6107.
(58) Hofmann, D.; Heuchel, M.; Yampolskii, Y.; Khotimskii, V.; Shantarovich, V. *Macromolecules* **2002**, *35*, 2129.
(59) Shimazu, A.; Miyazaki, T.; Ikeda, K. *J. Membr. Sci.* **2000**, *166*, 113.
(60) Dlubek, G.; Buchhold, R.; Hubner, C.; Nakladal, A. *Macromolecules* **1999**, *32*, 2348.
(61) Van Krevelen, D. W. *Properties of Polymers: their Correlation with Chemical Structure; their Numerical Estimation and Prediction from Additive Group Contributions*, 3rd completely revised ed.; Elsevier: Amsterdam, 1990.
(62) Hoy, K. L. *J. Paint Techn.* **1970**, *42*, 76.
(63) Fedors, R. F. *Polym. Eng. Sci.* **1974**, *14*, 147.
(64) Hofmann, D.; Fritz, L.; Ulbrich, J.; Paul, D. *Polymer* **1997**, *38*, 6145.
(65) Widom, B. *J. Chem. Phys.* **1963**, *39*, 2808.
(66) Müller-Plathe, F. *Acta Polym.* **1994**, *45*, 259.
(67) Neyertz, S.; Brown, D.; Douanne, A.; Bas, C.; Albérola, N. D. *J. Phys. Chem. B* **2002**, *106*, 4617.
(68) Kotov, B. V. *Russ. J. Phys. Chem.* **1988**, *62*, 1408.
(69) Salley, J. M.; Frank, C. W. In *Polyimides: Fundamentals and Applications*; Ghosh, M. K., Mittal, K. L., Eds.; 1996; p 279.
(70) Dinan, F. J.; Schwartz, W. T.; Wolfe, R. A.; Hojnicki, D. S.; Clair, T. S.; Pratt, J. R. *J. Polym. Sci.: Part A: Polym. Chem.* **1992**, *30*, 111.
(71) Ando, S.; Matsuura, T.; Sasaki, S. *Polym. J.* **1997**, *29*, 69.
(72) Wachsman, E. D.; Frank, C. W. *Polymer* **1988**, *29*, 1191.
(73) Viallat, A.; Bom, R. P.; Cohen-Addad, J.-P. *Polymer* **1994**, *35*, 2730.
(74) Graser, F.; Hädicke, E. *Liebigs Ann. Chem.* **1980**, , 1994.
(75) Graser, F.; Hädicke, E. *Liebigs Ann. Chem.* **1984**, , 483.
(76) Bondi, A. *Physical Properties of Molecular Crystals, Liquids and Gases*; John Wiley & Sons: New York, 1968.
(77) Yu, W. C.; Sung, C. *Macromolecules* **1988**, *21*, 365.
(78) Lee, S.; Mattice, W. L. *Comput. Theor. Polym. Sci.* **1999**, *9*, 57.
(79) Nagel, C.; Schmidtke, E.; Günther-Schade, K.; Hofmann, D.; Fritsch, D.; Strunkus, T.; Faupel, F. *Macromolecules* **2000**, *33*, 2242.
(80) Schmitz, H.; Muller-Plathe, F. *J. Chem. Phys.* **2000**, *112*, 1040.
(81) Bondi, A. *J. Phys. Chem.* **1964**, *68*, 441.
(82) Tamagna, C. Ph.D. Thesis, University Claude Bernard, Lyon, France, 1998.
(83) Hirayama, Y.; Yoshinaga, T.; Kusuki, Y.; Ninomiya, K.; Sakakibara, T.; Tamari, T. *J. Membr. Sci.* **1996**, *111*, 169.
(84) Kim, T. H.; Koros, W. J.; Husk, G. R.; O'Brien, K. C. *J. Membr. Sci.* **1988**, *37*, 45.
(85) Kim, T. H.; Koros, W. J.; Husk, G. R. *Sep. Sci. Technol.* **1988**, *23*, 1611.
(86) Hougham, G.; Tesoro, G.; Viehbeck, A. *Macromolecules* **1996**, *29*, 3453.
(87) Simpson, J. O.; St-Clair, A. K. *Thin Solid Films* **1997**, *308*−*309*, 480.

MA020942J